Oscillating grid mesocosm for studying oxygen dynamics under controlled unsteady turbulence

Sabrina Lucas, Frédéric Moulin, Katell Guizien

LIMNOLOGY
and
OCEANOGRAPHY: METHODS

ASLO

Limnol. Oceanogr.: Methods 14, 2016, 1–13

doi: 10.1002/lom3.10064

Oscillating grid mesocosm for studying oxygen dynamics under controlled unsteady turbulence

Sabrina Lucas,[1,2] Frédéric Moulin,[3] Katell Guizien*[1,2]
[1]CNRS, UMR 8222, LECOB, Observatoire Océanologique, Banyuls/mer, France
[2]UPMC Univ Paris 06, UMR 8222, LECOB, Observatoire Océanologique, Banyuls/mer, France
[3]Institut de Mécanique des Fluides de Toulouse, UMR 5502, Toulouse, France

Abstract

In shallow environments, common unsteady flows, such as tides, waves or wind-driven currents modulate the diffusive boundary layer thickness that controls the exchange of electron acceptors for mineralization and oxidation processes in surficial sediment. This study demonstrated the ability of an oscillating grid mesocosm to (1) produce homogenous turbulence at the sediment-water interface of multiple sediment cores (between-core variability < within core variability; 16% on average); (2) simulate diffusive boundary layer thickness dynamics on different timescales by easy control of turbulence intensity and (3) study transient oxygen dynamics of organic matter mineralization under varying turbulent conditions. The relationship between turbulence intensity and oxygen diffusive boundary layer thickness, and oxygen penetration depth in the sediment was investigated with different organic matter enrichments and sediment permeability. Oxygen diffusive boundary layer thickness decreased linearly as U_{RMS} increased. Oxygen penetration depth increased with turbulence intensity, and converging to an upper limit with a larger value for low (3.28 mm ± 5.8%) than for high (1.77 mm ± 11.8%) organic matter content in muddy sediment. In sandy sediment, advective flows and resuspension led to a continuous increase of oxygen penetration depth with turbulence intensity, up to 13.2 mm ± 19% for turbulent velocities of 9.6 cm s^{-1}. This mesocosm device will enable the experimental study of microbial dynamics under transient oxygen dynamics, to improve early diagenesis modeling under unsteady flows.

In shallow waters (rivers, coastal zones, or lagoons), organic matter (OM) accumulates in bed sediment after passing through the water column from the photic zone or watersheds. Particulate organic material falling at the sediment-water interface (SWI) modifies the chemical composition of the sediment and evolves during the so-called "early diagenesis." This process controls the biogeochemical cycle of carbon and others elements, such as nitrogen and sulfur (Froelich et al. 1979) through various biological (bioturbation and bacterial activity) and chemical (oxidation, precipitation) processes (Aller 1994). Moreover, this particulate OM mineralization contributes to the supply of carbon, nutrients and energy necessary for the metabolism of benthic organisms. Thus, the rate of degradation of OM in sediment is a key end-member for the carbon balance of the planet, because sedimentation rates greater than mineralization rates lead to a net sink of carbon through the storage of OM in impermeable sediments (Aller et al. 1996).

OM mineralization occurs mainly in surficial sediment, where it is limited by the rapid disappearance of oxygen with depth (Glud et al. 2005); generally, the richer the OM content in the sediment, the faster the oxygen disappears. This disappearance is due to the respiration of microorganisms associated with aerobic degradation of OM, and the oxidation of reduced compounds produced during anoxic degradation of OM (Canfield et al. 1993). At the SWI, the diffusive boundary layer (DBL) is a thin layer of fluid where molecular diffusion dominates and limits the transfer of dissolved material between the overlying water and the interstitial water in the sediment (Gundersen and Jorgensen 1990). Oxygen diffusive flux, from water column to sediment, is influenced by turbulence intensity (Boudreau and Jørgensen 2001) that controls the diffusive boundary layer thickness (δ_{DBL}); the higher the turbulence at the SWI, the thinner the diffusive boundary layer thickness (δ_{DBL}) and the faster the oxygen flux across the SWI (Steinberger and Hondzo 1999; House 2003; Glud et al. 2007).

At sea, gravity waves with time scales ranging from seconds (waves) to hours (tides) create oscillatory flows that dissipate most of their energy (75%) when the water depth decreases nearshore (Munk and Wunsch 1998; Thorpe 2005). Energy dissipation occurs in the benthic boundary layer,

*Correspondence: guizien@obs-banyuls.fr

where it displays alternately highly turbulent and laminar periods (Guizien et al. 2003), and creates an unsteady oxygen supply to the bed sediment ranging from seconds to hours (Chatelain and Guizien 2010). Other aperiodic unsteady flows, such as river floods or wind-buoyancy driven currents, can induce similar turbulent fluctuations near the bed causing oxygen supply to the sediment to vary over longer time scales, from days to weeks. Such fluctuations of oxygen supply to the sediment will cause fluctuations of oxygen penetration (δ_{O_2}) into the sediment, exposing the macro- and microbenthic communities to varying oxic conditions, which may affect their functioning (Gantzer and Stefan 2003; Higashino and Stefan 2005; Morse and Eldridge 2007).

Furthermore, energy dissipation of highly energetic flows such as storm swell will cause sediment erosion, which will be redeposited when flow energy decreases. Sediment resuspension has been demonstrated to increase the rates of exchange of solutes between the sediment and the water column, and to stimulate oxygen uptake because of enhanced microbial respiration rates (Fanning et al. 1982; Wainright and Hopkinson 1997). These resuspension events stimulate OM mineralization in suspension phase (Stahlberg et al. 2006), and also expose transiently the deep anoxic sediment layer to increased oxygen supply (Abril et al. 2010; Frindte et al. 2013), which may also enhance OM degradation in the eroded bed (Almroth et al. 2009).

Since the 1980s, many studies of OM mineralization have been carried out, in particular on the oxygen dynamics in the sediment (flux and consumption). The two methods used most commonly for determining oxygen uptake in sediments are: (1) laboratory measurements in sediment cores (Rasmussen and Jørgensen 1992), and (2) in situ measurements with benthic chambers, which isolate the surface sediment and overlying water (Glud et al. 1995; Tengberg et al. 1995, 2004; Almroth et al. 2009). In these two methods, the captured overlying water is maintained with a constant stirring different to the movement of natural flows. Thus, oxygen fluxes and consumptions are calculated in steady conditions, which do not reflect natural environments. In recent decades, an increasing number of studies using microelectrodes have confirmed that hydrodynamic fluctuations induce δ_{DBL} variations, which affect significantly the oxygen distribution (Lorke et al. 2003; Glud et al. 2009). The new non-invasive technique of eddy correlation measures in situ upward oxygen turbulent fluxes (correlation between turbulent fluctuations of vertical velocity and oxygen concentration), together with flow velocity (Berg et al. 2003). This technique has shown that measurements with benthic chambers underestimate oxygen fluxes because of the modification of the physical forcings (Berg et al. 2003). It has also provided evidence of the temporal variations of oxygen flux in relation to natural flow dynamics (Bryant et al. 2010a; Holtappels et al. 2011). However, one should question whether such temporal variations of oxygen flux reflect only the control of mass transfer at the SWI by the flow, or whether they also reflect changes in the respiration of micro- and macro-organisms of the sediment in response to changing environmental conditions. Indeed, niche theory states that species exhibit different optimal ranges of environmental conditions, which should favor their growth compared with other species (Hutchinson 1957). Consequently, environmental factor dynamics should translate into different population dynamics or at least different metabolism rates for species with different niches. However, characteristic time scales of population or activity decay, when environmental conditions evolve beyond the niche of the organism, are still poorly known. To achieve this goal, a step back into the laboratory is necessary to explore the relationship between respiration activity and/or population dynamics and controlled turbulence fluctuations at different field-relevant time scales. Such benchmark experimental data will be used to develop formulations of biological dynamics in response to the variability of local environmental conditions in diagenetic models (Gantzer and Stefan 2003; Higashino and Stefan 2005). To facilitate the mass production of such novel benchmark experiments, a standardized, affordable and easy-to-use experimental setup that ensures spatially uniform mass transfer control at the SWI, to provide replicability in both time and space, still has to be designed. Although flumes have been used extensively to evidence and investigate transport processes in sheared turbulent boundary layers created by flow above SWI (Kline et al. 1967), there are not accessible devices for most biogeochemists. Reproducing natural sheared turbulent boundary layer requires expensive large-scale facilities that are generally shared between many users with limited time of use while organic matter degradation experiment may last weeks or months. Alternative devices to control diffusive transfer across SWI that are easier to handle and smaller should be considered.

The aim of this article is to test the ability of a mesocosm, in which a purely diffusive and homogenous turbulence is generated by an oscillating grid, to: (1) produce homogenous control of diffusive flux at the SWI of multiple sediment samples; (2) simulate δ_{DBL} dynamics at different time scales by easy control of turbulence intensity and (3) study the transient oxygen dynamics of OM mineralization under unsteady δ_{DBL}.

Material and procedure

Turbulence production by an oscillating grid system: calibration

Figure 1 shows the experimental setup of an oscillating grid turbulence generation system. The grid is formed of crossed square bars ($m = 1$ cm) spaced by 4 cm (mesh size M) placed horizontally above sediment cores (8-cm inner diameter) in a water tank (0.60 × 0.60 × 0.51 m height). The assembly oscillates vertically driven by a motor rotating at a

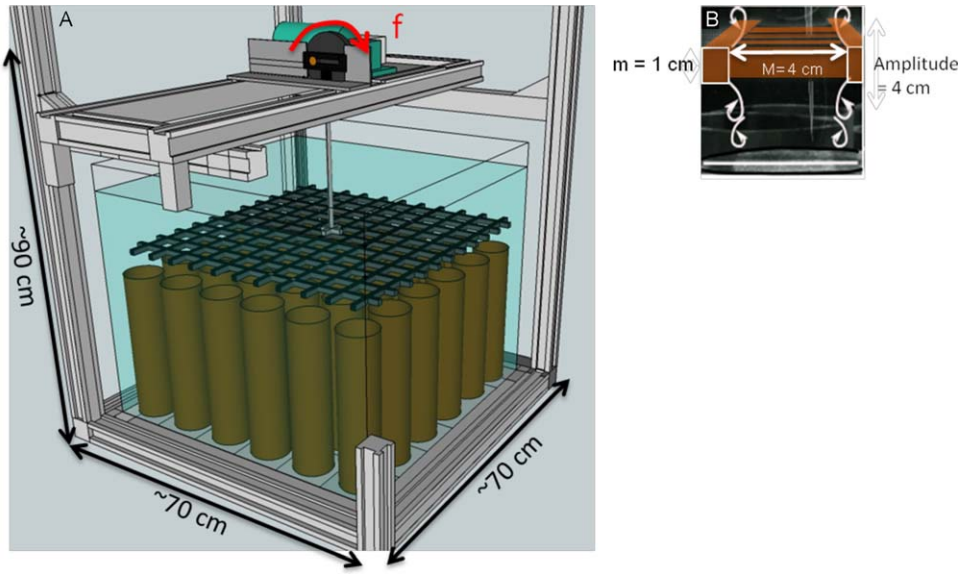

Fig. 1. (**A**) Experimental setup with oscillating grid above sediment cores. F represents frequency motor and S stroke length – (**B**) Grid parameters (*M*: mesh size; *m*: bar size). Arrows represent vortices produced by vertical oscillation of the grid.

frequency f, which ranges from 0.5 Hz to 3.5 Hz with a stroke length S (set mechanically with eccentricity). Thirty-six sediment cores were placed in a square configuration (6 × 6) at the bottom of a tank below the grid, to study early diagenetic processes under conditions of varying turbulence. Oscillating grid was used originally in theoretical studies of diffusive turbulence in stratified flows (Turner 1968; Hopfinger and Toly 1976), and more recently in suspension studies (Huppert et al. 1995; Medina et al. 2001). In a homogenous fluid, a vertical oscillating grid produces vortices, which diffuse and decay away from the grid, generating a locally turbulent flow. At 2.5 mesh lengths from the oscillating grid, the turbulence is purely diffusive, almost isotropic and laterally homogenous with a zero-mean flow. Such turbulence structure differs from the one of sheared boundary layer in which turbulence is produced at the SWI, decay away from it and is non-isotropic at the SWI with sweep ejections and large-coherent structures to which local advective processes are associated (Kline et al. 1967). However, isotropic but well-controlled turbulent conditions in the oscillating grid turbulence generator, although not mimicking natural sheared flow conditions, may prove to be useful to control diffusive fluxes at the SWI by setting turbulence intensity. Turbulence intensity decays away from the grid following an empirical law of the form:

$$U_{\mathrm{RMS}} = W_{\mathrm{RMS}} = CM^{0.5}S^{1.5}fz^{-n} \text{(Hopfinger and Toly 1976)} \quad (1)$$

where U_{RMS} and W_{RMS} are the root mean square of the turbulent velocity fluctuations in the horizontal and vertical directions, respectively; z is the distance from the mid-position of the grid; C is a constant depending on the grid geometry (being equal to 0.25), and $n = 1$ (Hopfinger and Toly 1976). Thus, turbulence intensity at the core surface could be set by varying motor frequency, stroke length, and/or distance between the grid position and the surface of the sediment cores.

Turbulence and mean flow calibration in the mesocosm were carried out for a stroke length of 4 cm and motor frequencies ranging from 0.5 Hz to 6 Hz with two complementary techniques: particle image velocimetry (PIV) and two-dimensional laser doppler velocimetry (2D-LDV) measurements.

The PIV measurements were performed in a 17 × 5 cm window to obtain a spatial view of the turbulent and mean-flow structures. A vertical laser sheet was generated by a double cavity pulsed 30 mJ Nd-Yag laser (Quantel Twin) emitting at 532 nm. The flow was seeded with 10 μm micro-glass beads. Particle images were recorded by a high-resolution (2048 × 2048 pixels) 14-bit CCD camera (PCO 2000). The spatial resolution of the flow was 0.086 mm/pixel. All image-pair acquisitions were performed at 10 Hz for a total of 1000 pairs for each grid frequency. Each image pair was processed using the direct spatial cross-correlation techniques with peak-locking reduction algorithms (Fincham and Delerce 2000). The correlation box size was 23 × 23 pixels in both planes (i.e., about 2 × 2 mm) with an overlap of 50% on the calculation grid. Laser Doppler Velocimetry (LDV) was used to obtain better statistics of the turbulent flow than obtained by PIV (higher spatial resolution and 10-min time series with a minimum of 10,000 events to achieve a better time convergence) along four vertical lines: three above the same core to quantify intra-core variability, and one above another core for the inter-core variability. Measurements were carried out every 5 mm between the 5 mm

Table 1. Sediment characteristics for all experiments – mNE: non-enriched muddy sediment; mE1 and mE2: enriched muddy sediment and sNE: non-enriched sandy sediment.

Name	Type	D_{50}	Porosity	%OM
mNE	Muddy	39 μm	0.59	2.5%
mE1	Muddy	39 μm	0.59	4%
mE2	Muddy	39 μm	0.59	5%
sNE	Sandy	172 μm	0.38	2.5%

below the lowest position of the grid and 5 mm above the core surface.

Experimental treatments

Muddy and sandy marine sediment cores, sieved at 200 μm to avoid non-local oxygen consumption by bioturbation processes, were constructed and left to consolidate for a minimum of 7 d. Two days before the turbulence experiment, the upper 2 cm of some muddy sediment cores was homogenized and enriched with lyophilized fish meat, yielding two different OM contents. OM content, porosity and grain size were assessed over the first 0.5 cm for the four experimental treatments (non-enriched muddy (mNE), two enriched muddy (mE1 and mE2), and non-enriched sandy (sNE)—Table 1).

The weight of the OM content was assessed by loss-on-ignition after sequential heating of the samples in a muffle furnace (Dean 1974) using the following equation:

$$\mathrm{OM\%} = ((\mathrm{DW}_{105} - \mathrm{DW}_{450})/\mathrm{DW}_{105}) \times 100 \quad (2)$$

where OM% denotes the loss-on-ignition at 450°C, DW_{105} is the dry weight after drying at 105°C for 24 h, and DW_{450} is the dry weight of the sample after heating to 450°C for 4 h (both in g). Sediment porosity (ϕ) was also assessed according to Manheim and Waterman (1974) using the following equation:

$$\Phi = \frac{(\mathrm{WW}_4 - \mathrm{DW}_{60})/\rho_w}{((\mathrm{WW}_4 - \mathrm{DW}_{60})/\rho_W) + ((\mathrm{DW}_{60} - \mathrm{TW})/\rho_w)} \quad (3)$$

where ρ_w denotes pore-sea water density (1.025 g cm^{-3}), ρ_s denotes sediment density (taken equal to 2.65 g cm^{-3}), WW_4 is the wet weight of the sample at 4°C, DW_{60} is the dry weight of the sample after drying at 60°C for 72 h, and TW is the tare weight of the cup. Sediment grain-size distribution was measured with a laser grain-size analyzer Mastersizer 2000 (Malvern) and was unimodal for both the muddy ($d_{50} = 39$ μm) and sandy sediments ($d_{50} = 172$ μm, Table 1).

Then, the cores were positioned at 7.5 cm from the mid-position of the grid in the muddy sediment experiment and at 4.6 cm from the mid-position of the grid in the sandy sediment experiment. Turbulence intensity above the sediment cores interface was varied by increasing the motor frequency from 0 Hz to 3 Hz in steps of 0.5 Hz and described by U_{RMS} values of the power fit law established in turbulence calibration experiment at a distance of 2 cm above the sediment core which corresponds 5.5 cm (resp. 2.6 cm) from grid mid-position in muddy (resp. sandy) experiment. At such a distance from sediment-water interface, turbulence intensity is expected to be measured outside the boundary layer that develops above the sediment-water interface.

Oxygen dynamics measurements

During each experiment, oxygen profiles were carried out with microelectrodes (OX10fast, Unisense A/S – Revsbech 1989) every 20 min around the SWI (from −2 cm in the water to +2 cm in sediment with steps of 200 μm) throughout the experiments at the same location (center or on the edge) in three different cores. Oxygen microelectrodes were calibrated using the signal reading in the water column (100%) and in the anoxic part of the sediment (0%).

To determine the SWI position in the oxygen profiles, two methods were used. The first method consisted of detecting the SWI visually with the microelectrode tip and setting this position as a zero vertical coordinate for subsequent oxygen profiles. The second method consisted of defining the SWI as a discontinuity in the slope of the oxygen profile (Boudreau and Jørgensen 2001). Indeed, porosity displays a jump from a value of 1 in the water to a value below 1 in the sediment, and diffusivity in the sediment is lower than the molecular diffusivity in the water. As oxygen diffusive flux is continuous across the SWI, this jump of porosity leads to a jump in the slope of the oxygen profile. The ratio of oxygen slopes above and below the SWI is equal to the ratio of the porosity divided by the square of the tortuosity:

$$\frac{\partial \mathrm{O}_2}{\partial \mathrm{z}^+} \Big/ \frac{\partial \mathrm{O}_2}{\partial \mathrm{z}^-} = \frac{\Phi}{\theta^2} \quad (4)$$

According to Ullman and Aller (1982), $1/\theta^2 = \Phi^{m-1}$ where $m = 2$ when $\Phi < 0.7$, and therefore, the ratio of the oxygen slopes across the SWI should be close to the square of the porosity. This second method was assessed on the muddy cores by comparing successfully the SWI position detected visually to that defined by the oxygen slope break with a slope ratio close to 0.35 (around Φ^2 as $\Phi = 0.59$). In the sandy sediment experiment ($\Phi = 0.38$), when turbulence intensity was large enough to generate a resuspension of non-cohesive particles with median grain size of 172 μm, the SWI started to move during the experiment. Thus, the SWI position was calculated using the second method for each oxygen profile.

Determination of diffusive boundary layer thickness and oxygen penetration depth

Intercomparison of the different methods used to determine the diffusive boundary layer thickness (δ_{DBL}) revealed

that some methods were not universal because of the rapid variation of turbulence in the natural environment (Lorke et al. 2003; Roy et al. 2004; Brand et al. 2009). Moreover, several methods are sensible to the position of SWI that may be poorly defined (i.e., in the field); for example, when SWI position was higher than estimated, δ_{DBL} would have been underestimated (Bryant et al. 2010b). Such a limitation is reduced significantly in the laboratory where precise positioning of the probe is achievable. In this study, δ_{DBL} was defined by two methods: the linear and the 95% method. By definition, the DBL is the zone in which molecular diffusion dominates and hence turbulent diffusion is negligible. In this zone, under the assumption of steadiness, no consumption of oxygen in the water and no advective flow, mass balance of oxygen yields a linear decay of oxygen concentration within the DBL (Jorgensen and Des Marais 1990). Therefore, the DBL was detected during steady period at the end of each turbulence step as the part of the oxygen profile above SWI where correlation coefficient of linear regression between oxygen concentration and distance to SWI was superior to 0.975 with a *p*-value inferior to 0.05. However, the linear method ($\delta_{DBL\ linear}$) (Jorgensen and Des Marais 1990) is not be applicable in a transient regime when turbulent diffusivity is not constant (Roy et al. 2004). The alternative 95% method was thus used to estimate DBL thickness ($\delta_{DBL\ 95\%}$) along the entire experiment, including transient periods. The 95% DBL thickness is the distance between the SWI and the elevation where 95% of oxygen saturation was reached in the vertical oxygen profiles. Such a definition facilitates comparison with results from numerical models in which the δ_{DBL} has been similarly defined by a percentage of oxygen saturation (99% in Higashino et al. 2004; Chatelain and Guizien 2010). However, because the precision of the microelectrodes was only 2%, the use of the 99% level of oxygenation was too imprecise; therefore, the 95% level of oxygen saturation was chosen. Other alternative methods were not relevant for this mesocosm, in particular, the friction velocity method (Hondzo et al. 2005; O'Connor and Hondzo 2008) based explicitly on sheared turbulence production, which does not apply in a system with purely diffusive turbulence.

Symmetrically, the oxygen penetration depth (δ_{O_2}) was defined as the distance between the SWI and the elevation where a 5% level of oxygen saturation was reached in the vertical oxygen profiles.

Temporal, spatial and spatio-temporal variabilities in δ_{DBL} and δ_{O_2} were estimated for each turbulent intensity in all experiments. Temporal variability was defined as the mean of the three cores standard deviations along a turbulent step. Spatial variability was defined as the mean along a turbulent step of the standard deviations between the three cores. Spatio-temporal variability was defined as the standard deviation along a turbulent step and between the three cores. All statistical analyses were performed using MATLAB® with an analysis of means (*t*-test), linear regression and Pearson's correlation test.

Assessment

Assessment of turbulence intensity control and its spatial variability

PIV measurements yielded a spatial view of the turbulent and mean-flow structures in a vertical plane below the grid and above two adjacent cores (Fig. 2A). Higher turbulence energy below the grid, where vortices detached, displayed the spatial periodicity in turbulence production imposed by the grid mesh size. Spatial variability due to turbulence production strongly decreased at a distance of around one mesh grid. Cores geometry did not create significant spatial variability in the turbulence field, but core presence constrained a mean recirculating flow between the grid and surface of the cores, which displayed a dominant periodicity at grid mesh size. In the present study, the distance between the surface of the cores and the grid mid-position was less than 9 cm, to enable micro profiling given the design of the mounting of the microelectrodes. As this distance was less than 2.5 times the mesh size, a non-zero mean-flow was still present, turbulent at the surface of the cores as shown on Fig. 2A. However, near the cores and for all motor frequency velocities U_{RMS} dominated, on average, by a factor of two the value of the mean-flow, as spatial variations of this factor ranged from 1.25 to 5 along a core cross section. The thickness of the diffusive boundary layer was thus controlled mainly by turbulent processes, as would have been expected had zero mean-flow conditions been obtained, and to a lesser extent, by its development along the external advective flow.

Root mean square of the turbulent velocity fluctuations in the horizontal (Fig. 2B) and vertical (Fig. 2C) directions display the expected decay away from the grid. Turbulence intensity was more different between the center (low intensity) and the border (high intensity) of a core than between the center of two different cores, and intra-core spatial variability increased with motor frequency (Fig. 2B,C). This variability resulted from the spatial periodicity of turbulence production imprinted by the grid mesh size which was nearly equal to the core radius, and thus also matched cores spacing. A power law ($a\ Z^{-n}$) was fitted on four profiles measured above two cores for motor frequencies ranging from 0.5 Hz to 3.5 Hz, and on a single profile measured in a center of a core for frequencies of 4 Hz, 5 Hz, and 6 Hz (Table 2). Fitting on a single profile yielded a residual error lower than 4%, while fitting on four profiles was much less accurate, with residual error up to 25%. In presence of cores, exponent values for the power law varied from 0.58 to 1.83, averaging at 1.08 (Table 2), thus deviating by 8% from the exponent of 1 found by Hopfinger and Toly (1976) in an empty tank, without cores. Deviation from the exponent of 1 is likely due to the turbulence intermittency produced by unsteady vortex shedding in the near grid field (Chien et al. 2013) as the power law fitting was performed

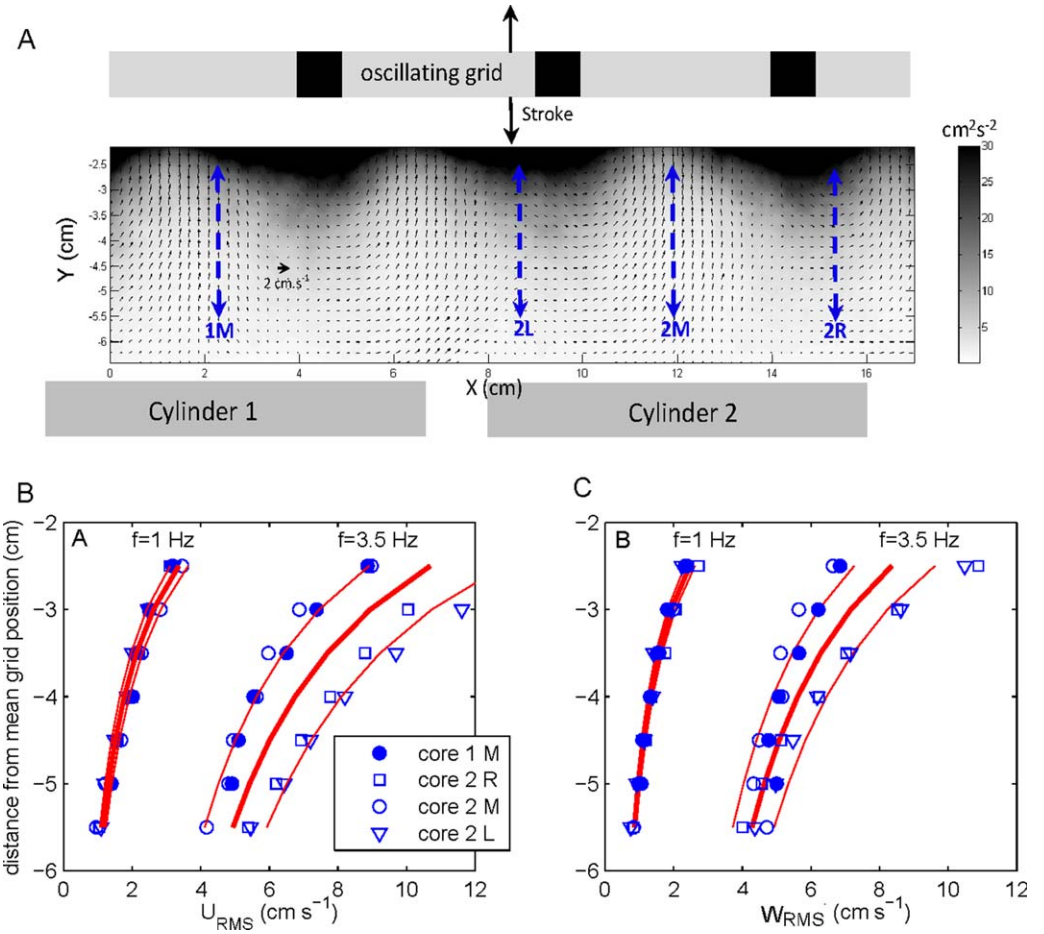

Fig. 2. (**A**) Turbulent kinetic energy (grayscale in $cm^2\ s^{-2}$) and mean flow (every two points, arrows indicate flow direction and their length is proportional to flow speed) below the oscillating grid (transverse bars are shown by filled black squares) and above cores interface (displayed by grey rectangles) for a stroke of 4 cm and motor frequency of 3.5 Hz. The position of the four locations (1M, 2M, 2L, 2R) where LDV profiles were performed are displayed. Vertical profiles of U_{RMS} (**B**) and V_{RMS} (**C**) under the grid in the middle of two different cores (core 1 M and core 2 M), and left (core 2 L) and right (core 2 R) of one of the two cores for a stroke of 4 cm and for two motor frequencies of 1 Hz and 3.5 Hz. Thick lines display the power law best fit carried out after grouping the four profiles and thin lines display the variability interval defined by the best fit residual error for each motor frequency.

closer from grid mid-position (between 0.5 and 1.5 mesh size, due to the constrained space between grid and cores) than in previous experimental studies (Hannoun and List 1988; Redondo 1988; Fernando 1991) which validated the exponent of 1 beyond at least one mesh size away from the grid. Spatial heterogeneity of the flow statistics due to turbulence intermittency within or between cores was estimated by the residual error of the power law fitting and averaged at 16% for motor frequencies ranging from 0.5 Hz to 3.5 Hz among the four profiles. To ensure minimal variability in turbulence conditions in profile replicates, oxygen profiling was systematically carried out in the middle of the grid void that were located above core centers. In addition, turbulence intermittency at the cores SWI was reduced as the cores were placed beyond 2 mesh sizes away from the grid mid-position.

Diffusive boundary layer thickness controlled by oscillating grid turbulence

Short experiments consisted of increasing the turbulence intensity stepwise (six steps) from stagnant water to high turbulence conditions ($U_{RMS} = 4$ cm s^{-1} at 2 cm above the SWI in muddy experiments and 9.6 cm s^{-1} at 2 cm above the SWI in sandy experiment), the end of each step being defined by the moment in which steady oxygenation of either the muddy or sandy sediment was reached (2 h approximately). Figure 3 shows the evolution of $\delta_{DBL\ 95\%}$, $\delta_{DBL\ linear}$ recorded by one sensor throughout the experiments for muddy sediment with low OM content (Fig. 3A) and high OM content (Fig. 3B). $\delta_{DBL\ linear}$ was only calculated for the low OM content at the end of each turbulence step during the steady period (Fig. 3A), when oxygen profiles were linear near the sediment-water interface (Fig. 3C). For

Table 2. Coefficients (a, n) of power law ($a\ Z^n$) best fit of the U_{RMS} profiles measured with the LDV in four locations above two cores (bold, locations are defined in Fig. 2A) or along one profile only in the center of a core (not bold) for motor frequencies ranging from 0.5 Hz to 6 Hz. The residual error of the best fit (denoted σ) is given in percentage.

Motor frequency (Hz)	a	n	σ (%)
0.5	**7.44**	**1.83**	**16.5**
1	**11.7**	**1.36**	**8.0**
1.5	**10.7**	**0.95**	**24.5**
2	**13.6**	**1.00**	**17.9**
2.5	**19.8**	**1.02**	**23.3**
3	**29.5**	**1.17**	**3.6**
3.5	**26.2**	**0.98**	**20.0**
4	37.6	1.21	4.0
5	18.4	0.67	2.1
6	18.3	0.58	1.5

the high OM content, $\delta_{DBL\ linear}$ could not be calculated during steady periods as oxygen profiles were parabolic near the sediment-water interface (Fig. 3D). Such parabolic profile denotes oxygen consumption in water probably due to the chemical oxidation of the reduced compounds diffusing from the sediment where it accumulated after organic matter mineralization. When turbulence intensity increased, both estimates of δ_{DBL} decreased, although $\delta_{DBL\ linear}$ were always lower than $\delta_{DBL\ 95\%}$. $\delta_{DBL\ 95\%}$ converged to almost the same value (1.1 mm $\pm$ 18%, average value +/− standard deviation of the three sensors) when turbulence intensity was increased, in the two sediment enrichment treatment. Transient periods duration varied differently with turbulent intensity in the low and high OM enrichment conditions. Transient period duration decreased when turbulence intensity increased at low OM content (Fig. 3A) whereas transient period duration increased with turbulence intensity at high OM content (Fig. 3B). Consequently, experiments lasted about 12 h for low OM content and 16 h for high OM content.

In the experiment at low OM content, where δ_{DBL} could be estimated with the linear method, $\delta_{DBL\ linear}$ (average value +/− standard deviation of the three sensors along the steady turbulent period) decreased from $1.4 \pm 14\%$ mm down to $0.7 \pm 24\%$ mm when turbulence intensity increased from $U_{RMS} = 0.3$ up to 4 cm s^{-1} (Fig. 4A), as a result of the enhancement of oxygen water-side diffusive flux with

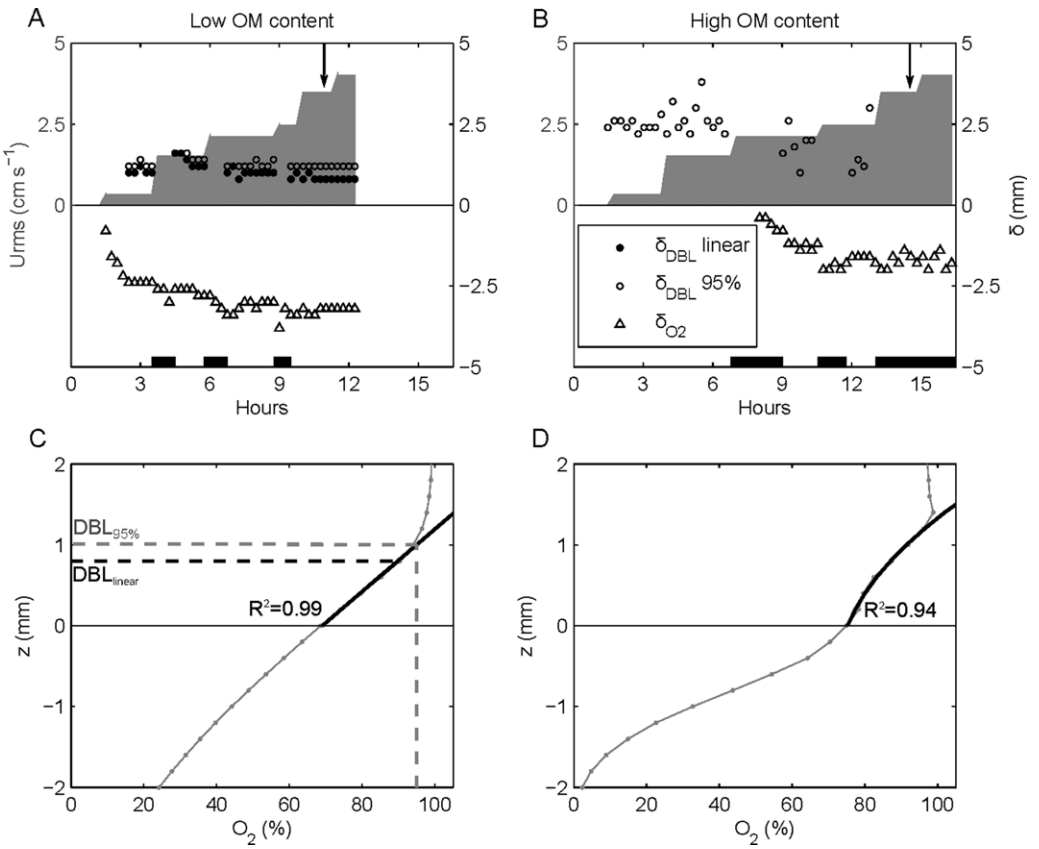

Fig. 3. Evolution of $\delta_{DBL\ linear}$ (black points), $\delta_{DBL\ 95\%}$ (white points) and δ_{O_2} (triangle) during short experiments for muddy sediment with low OM content (**A**) and high OM content (**B**). Turbulence steps are represented by grey areas and transient periods duration are represented by black line. **C** and **D** represent one oxygen profile at sediment-water interface during stationary (**C**) and transitory regime (**D**).

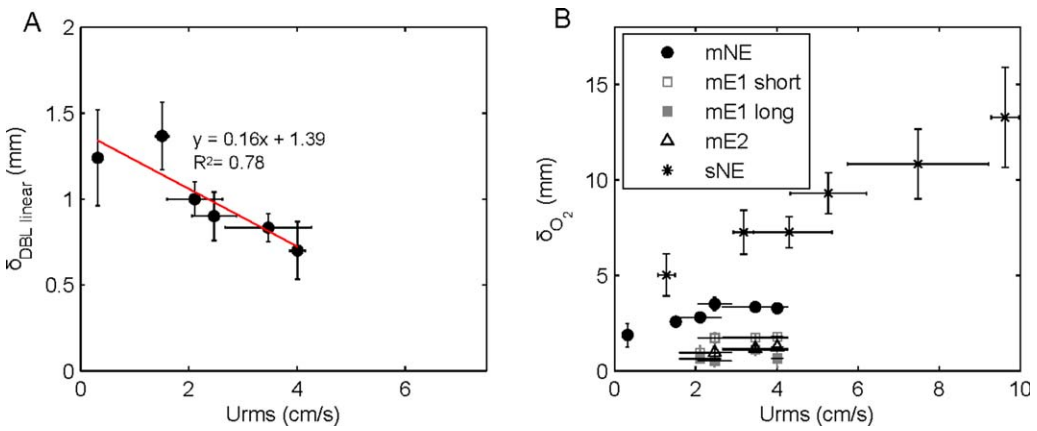

Fig. 4. Evolution of $\delta_{DBL\ linear}$ (**A**) and δ_{O_2} (**B**) with turbulence intensity (Urms) for all sediments (black points: non-enriched muddy, white squares: enriched muddy and stars: non-enriched sandy).

turbulence in steady conditions of low sediment respiration. Moreover, a linear regression fit between $\delta_{DBL\ linear}$ and U_{RMS} at 2 cm above SWI was significant ($R^2 = 0.78$, p-value = 0.018*). Such linear decay of $\delta_{DBL\ linear}$ when U_{RMS} increased provides a uniform control of diffusive fluxes from low flow to high flow conditions in the oscillating grid turbulence generator. At high OM content, δ_{DBL} estimated from 95% limit also decreased when turbulence intensity increased, demonstrating that oscillating grid mesocosm controls diffusive boundary layer thickness.

Other laboratory experiments and numerical models (Steinberger and Hondzo 1999; House 2003; Higashino et al. 2004) have studied the effect of turbulence on the oxygen mass transfer above artificial and natural porous-media-water interfaces. In these studies, turbulence produced by sheared flows in flumes was quantified as friction velocity. Controlling diffusive fluxes at low flow conditions would be less precise in flume facilities compared with the oscillating grid mesocosm, as in sheared flows, δ_{DBL} is inversely proportional to the friction velocity (Dade 1993), thus to U_{RMS}. Yet, direct comparison of δ_{DBL} vs. turbulence intensity is not possible, owing to the different nature of the turbulence production mechanism between a sheared flow and an oscillating grid (Redondo et al. 2001). However, the relationship between δ_{DBL} and oxygen concentration at non-permeable SWIs found in these studies, can be compared with this study because this relationship only results from the balance between oxygen consumption in the sediment and oxygen diffusion across the SWI in an infinite water depth (Gundersen and Jorgensen 1990; Glud et al. 2007).

Relative oxygenation of the SWI vs. δ_{DBL} for the non-enriched muddy sediment of this study (oxygen consumption rate was about 100 mg L^{-1} d^{-1}, calculated from general equation of early diagenesis, Berner (1980) was compared with Steinberger and Hondzo's experimental data (1999) and with the numerical simulations of Higashino et al. (2004) for two oxygen consumption rates (100 mg L^{-1} d^{-1} and 1000 mg L^{-1} d^{-1}, Fig. 5). Data from a field study exhibiting the oxygen dynamics across the SWI during an 8 h seiche-cycle in a mesotrophic lake were also reported (Bryant et al. 2010b). All results indicated SWI oxygenation when the δ_{DBL} decreased, although with different relationships between SWI oxygenation and δ_{DBL} thickness. Large difference arose from methods of determination of the δ_{DBL}: much larger δ_{DBL} thickness estimates were found in Higashino et al. (2004), which used a definition based on 99% of oxygen saturation. In comparison to the direct method δ_{DBL} estimates based on the slope of the vertical oxygen profiles at the SWI that was used in the present experimental study, the 99% method mimicked an increase of oxygen consumption rates

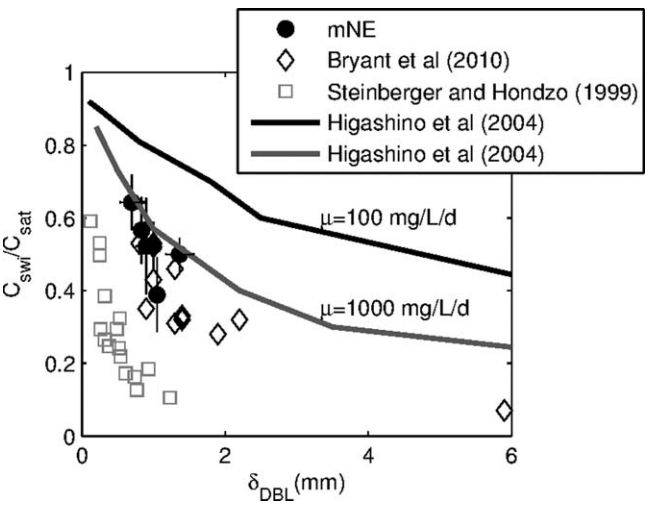

Fig. 5. Relation between C_{swi}/C_{sat} and δ_{DBL} for all sediment types. Black points represent $\delta_{DBL\ linear}$ of non-enriched muddy sediment. Squares represent Steinberger and Hondzo's data (1999) and diamonds represent Bryant's et al. (2010b) data; Black and grey lines represent oxygen consumption in the paper of Higashino et al. (2004).

by a factor 10. Still, although δ_{DBL} thickness was estimated with the same method in the experimental and field studies, different curve slopes were observed, reflecting different oxygen consumption rates. Higher levels of enrichment and possibly higher lability of sugars used in Steinberger and Hondzo (1999) study yield lower SWI oxygenation compared with this study in which less labile fish meat proteins were used. Indeed, as indicated by numerical simulations, the higher the consumption rate, the larger the SWI oxygenation decay when δ_{DBL} thickness increases. Similarly, SWI oxygenation decayed less rapidly when δ_{DBL} thickness increased in Bryant et al. (2010b) data than in Steinberger and Hondzo's (1999) experimental data, which reflects the lower lability of terrigenous OM in a mesotrophic lake compared with sugar enrichment. The SWI oxygenation in this study were close enough to Bryant et al. (2010b) data to establish the natural representativity of the artificial enrichment of this study. Moreover, large δ_{DBL} values observed in Bryant et al. (2010b) indicated that low turbulence conditions occur in the field. The present oscillating grid mesocosm was able to produce controlled diffusion rates low enough to mimic such low flow conditions, in contrast to flumes, in which steady low flows are less easy to reproduce (Steinberger and Hondzo 1999).

Yet, care should be taken at low flow conditions to avoid artefactual anoxia as happened in the enriched treatment of this study: a low turbulence below $U_{RMS} = 1$ cm s^{-1} was not sufficient to oxygenate the overlying water just above the sediment (Fig. 3B). Such depletion in water oxygenation evidenced consumption in the water column, probably due to upward diffusive flux of reduced compounds from the sediment into a limited water depth. Such an effect of the diffusion of reduced compounds from the sediment to the overlying water is damped in a flume where water is renewed (Steinberger and Hondzo 1999), but could be overcome in the oscillating grid mesocosm by increasing the water depth above the cores.

Oxygen penetration depth (δ_{O_2}) controlled by turbulence in non-permeable sediment: diffusion limitation

In parallel to DBL thickness decrease, oxygen penetration in the sediment increased with turbulence intensity, and converged to steady state (3.28 mm ± 5.8% average value of the three sensors throughout an entire turbulence stage including its spatio-temporal variability) for $U_{RMS} = 4$ cm s^{-1} at low OM content (Fig. 3). In non-permeable muddy sediment (oxygen transfer occurs through diffusion only), oxygen penetration depth increased rapidly with turbulence intensity as long as water-side diffusive flux remained limiting, i.e., lower than consumption rate. When water-side flux was no longer limiting as turbulence intensity increased, the increase of oxygen penetration depth slowed down, as sediment-side flux became limiting (Higashino et al. 2004). Lower consumption rate in the low OM content experiment explains that δ_{O_2} stabilized at lower turbulence intensity than in the higher OM content where higher consumption rate is expected (Fig. 3A,B). Moreover, oxygen penetration depth was the double in the low OM content experiment ($\delta_{O_2} = 3.3$ mm ± 5.8%) compared with the high OM content experiments ($\delta_{O_2} = 1.8$ mm ± 11.8% at OM = 4% and $\delta_{O_2} = 1.3$ mm ± 24.5% at OM = 5%), as a result of the equilibrium between sediment-side oxygen diffusion and different consumption rates (Fig. 4B).

In all experiments, spatial variability dominated over temporal variability along each turbulent intensity step by a factor of three for δ_{O_2}. Thus, values of spatio-temporal variability, reported in the text as standard deviations around the mean, reflect mainly the spatial variability. In muddy sediment, the relative standard deviation of δ_{O_2} (Fig. 4B) was larger at high OM contents than at low OM content ($t = -3.1753$, df = 6.033, p-value = 0.019) and decreased with turbulence intensity in both enrichment conditions (from 12% to 41% at OM = 4% and from 17% to 33% at OM = 5%). The variability of δ_{O_2} between cores in the oscillating grid mesocosm accounts for variability arising from either sedimentary oxygen demand variability or flow inhomogeneity. The latter was on average 16% (maximum 25%) and can by itself explain the variability of δ_{O_2} at high turbulence intensity. Meanwhile, at low turbulence intensity, variations in δ_{O_2} indicate variations in sediment oxygen demand, confirming the importance of replication inside the mesocosm to establish relationship between bulk descriptors.

Oxygen penetration depth (δ_{O_2}) controlled by turbulence in permeable sediment: advection and resuspension processes

In the sandy sediment experiment with low OM content, δ_{O_2} increased steadily with turbulence intensity ($R^2 = 0.97$ – p-value = 0.0005). At $U_{RMS} = 4.3$ cm s^{-1}, δ_{O_2} in sand is a double value ($\delta_{O_2} = 7.3$ mm ± 11%) than in mud ($\delta_{O_2} = 3.28$ mm ± 5.8%). At the maximum turbulent intensity ($U_{RMS} = 9.6$ cm s^{-1}), δ_{O_2} yielded 13.2 mm ± 19%. The coefficient of variation of δ_{O_2} did not show any significant correlation with turbulence intensity ($R^2 = -0.03$ – p-value = 0.86), and averaged at 16.2%. Yet, δ_{O_2} standard deviation increased with turbulence intensity ($R^2 = 0.79$ – p-value = 0.048). The variability in δ_{O_2} could be related to the variability of the relative position of the microelectrodes along the ripple in each core and thus, reflected the spatial structure of topography-driven advective flows (Huettel et al. 1996—Fig. 6A,B). Permeable sediments are characterized by high permeability and the presence of advective flows which dominates over molecular diffusion and facilitates sediment-water exchange of solutes and particles. Advective flows in permeable sediments are caused by a pressure gradient at the SWI, and they affect the pore water composition and its residence time. A spatially variable pressure gradient appears when flows interact with topography, which induces flow circulation in permeable sediments (Huettel and Gust 1992; Huettel et al. 1996). In our mesocosm, vortices generated at

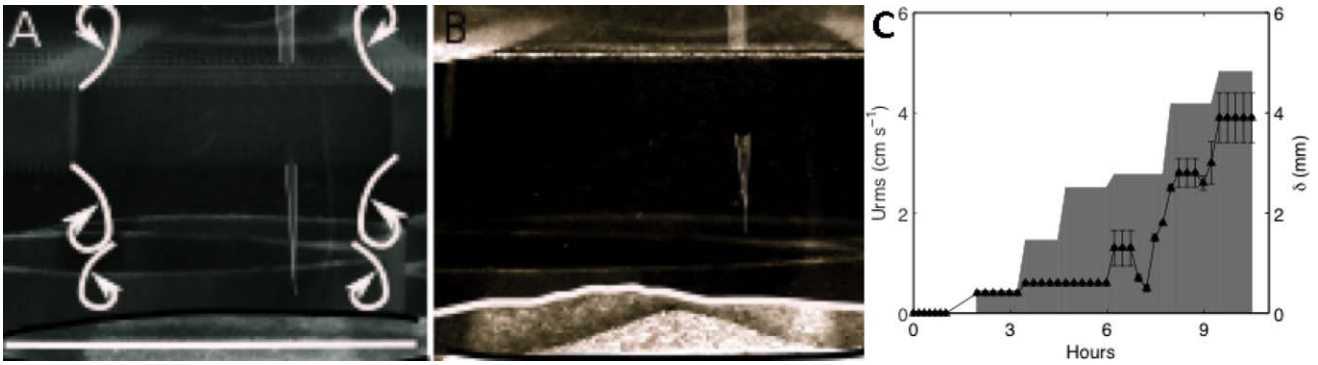

Fig. 6. Evolution of sediment-water interface position between the beginning (**A**) and the end of the experiment (**B**) for sandy sediment. White line: interface position. (**C**) Represents relative position of the sediment-water interface during experiment.

each grid oscillation interacted with the SWI and caused a mean recirculation downward below each bar of the grid and upward in the grid void. Such a circulation, together with turbulence energy sufficiently high to lift non-cohesive sand grains of 172 μm, leads to the formation of ripples at the SWI in the cores. The higher the turbulence level is, the larger the ripple height at the surface sediment cores.

Application perspectives of oscillating grid diagenetic mesocosm

With the present system, the turbulence level can be varied easily and rapidly as it responds linearly to oscillation frequency, enabling the reproduction of the temporal variability of turbulence that can be observed in natural flows (seiches, tides...). Unsteady flows occur recurrently in coastal waters, but in many studies (numerical, experimental and in situ), steady conditions have been applied in benthic chambers to calculate oxygen fluxes. Moreover, as benthic chambers deployed in the field disturb the flow conditions of the water, microbial activity dynamics in sediment may evolve to different states without reflecting the natural conditions (Glud et al. 1995; Tengberg et al. 1995).

Unsteady flows induce transient fluxes in oxygen supply at the SWI. This transient regime was evidenced in field studies by eddy-correlation and microprofiler (Lorke et al. 2003; Bryant et al. 2010a). However, extensive field deployments required to cover the range of time scale variability present in natural flows might be limiting. In broadening the range of unsteady flow conditions, numerical studies that rely on quasi-steady descriptions of flow turbulence, have shown that transient regimes, following shifts between turbulent and laminar conditions, could last several hours (Higashino et al. 2004). Numerical studies have also shown that transient phase duration decreases when turbulence and/or consumption rate increases (Higashino et al. 2004; Roy et al. 2004). These features were only partly confirmed by this study, where the time to reach steady state, following each turbulence step increase, decreased linearly from 60 min (for $U_{RMS} = 1.5$ cm s^{-1}) to 15 min (for $U_{RMS} = 2.5$ cm s^{-1}) in non-enriched sediment (Fig. 3A).

Recently, simulations carried out with a diffusion-reaction model, describing oxygen dynamics around the SWI, coupled with an oscillatory turbulent boundary layer model, showed that hysteresis in turbulence dynamics was amplified in diffusive flux dynamics across the SWI. This is because of the competition between the oxygen diffusion time across the diffusive boundary layer and the characteristic time of the δ_{DBL} dynamic and oxygen consumption time in the sediment (Chatelain and Guizien 2010). Moreover, in all these numerical simulations, oxygen consumption was modeled by assuming local adaptation to oxygenation conditions, hence disregarding the inherent dynamics of biological communities. For instance, the generation time of microbial organisms can vary from 30 min to several hours depending on environmental conditions, such as temperature, pH, salinity, redox potential, and oxygenation (Bissett et al. 2007; Edlund et al. 2008). Thus, transient oxygen supply controlled by unsteady flows could be expected to induce a dynamical response in microbial community respiration because of differential growth between microorganism populations. In the short experiments of this study, we intended to reduce the relative importance of microbial population dynamics vs. the turbulence changes by reducing the experiment duration. Meanwhile, transient duration was multiplied by a factor of three in the enriched sediment compared with non-enriched sediment, contradicting the decay of transient duration with increases of oxygen consumption (Higashino et al. 2004) and therefore, suggesting oxygen consumption decreased along the experiment. A complementary experiment was performed in which the same turbulence step increase (U_{RMS} ranging from 0.3 cm s^{-1} to 4 cm s^{-1}) was separated by longer stagnant periods of 2 d for the muddy sediment with an OM content of 4%. During turbulent periods, δ_{O_2} increased with turbulence intensity from $0.6 \pm 26\%$ to 1.1 mm $\pm 25\%$ when U_{RMS} increased from 2.1 cm s^{-1} to 3.5 cm s^{-1}, but decreased to 0.6 mm $\pm 70\%$ for $U_{RMS} = 4$ cm s^{-1}. In addition, although with similar enrichment at the beginning of experiment, δ_{O_2} was systematically lower in the long compared with the short time experiment (Fig. 4B). Moreover, these differences did not

exhibit a consistent trend throughout the experiment, as would be expected from the increasing difference in OM content following higher degradation in the long experiment compared with the short one. These results advocate for the inclusion, in unsteady early diagenesis numerical models, of an additional degree of liberty in respiration dynamics under the constraint of the intrinsic inertia of the microbial network. The mesocosm of this study, in which both physical and chemical diagenesis stratification are preserved, will facilitate experiments dedicated to developing and testing the validity of such formulation of microbial population respiration in response to local environmental dynamics.

Comments and recommendations

Although diffusive turbulence do not reproduce the structure of turbulence at sediment-water interface that is observed in natural sheared boundary layers, the present oscillating grid mesocosm has multiple advantages for the study of biogeochemical processes in various sedimentary environments (rivers, lagoons, fjords, deltas/estuaries, etc.) under unsteady diffusive boundary layer thickness:

1. production of controlled and fine-tuned diffusive boundary layer thickness with limited mean flow;
2. resuspension of non-cohesive sediment
3. easy monitoring of oxygen (and other compounds) with microelectrodes through the voids of the grid;
4. good replicability of turbulence conditions over 36 sediment cores, which permits the study of OM mineralization and microbial population dynamics; small size, easy of operation, dismantling and transport, which enables ex situ uses, even in remote locations.

Nevertheless, further improvements in the mounting of the microelectrodes would be necessary to increase the distance between the grid and the surface of the cores to reduce even further the flow convective cells. On the contrary, one may will to conserve flow convective cells to produce controlled bedforms at the SWI of non-cohesive sediment, adjusting grid mesh and sediment core sizes. Moreover, anoxic conditions were rapidly observed with enriched sediments displaying a high oxygen demand because of limited water volume in the experimental system. This limitation can be overcome by increasing the water height above sediment cores and using superposed grids in the tank to ensure continuity of turbulent transfer from the free surface to the SWI. Finally, the main limitation of the current mesocosm is the difficulty to resuspend cohesive sediment without shearing.

To conclude, the present mesocosm is a promising tool with which to perform benchmark experiments investigating the coupling between microbial community dynamics and diffusive boundary layer thickness fluctuations, which occurs in coastal waters with different periods and intensities (tides, waves, seiches).

Such experiments will facilitate the development of formulations of respiration dynamics in response to natural flow variability in diagenetic models, and improve the quantification of a key end-member of the earth carbon balance in the coastal zone.

References

Abril, G., and others. 2010. In vitro simulation of oxic/suboxic diagenesis in an estuarine fluid mud subjected to redox oscillations. Estuar. Coast. Shelf Sci. **88**: 279–291. doi:10.1016/j.ecss.2010.04.003

Aller, R. C. 1994. Bioturbation and remineralization of sedimentary organic matter: Effects of redox oscillation. Chem. Geol. **114**: 331–345. doi:10.1016/0009-2541(94)90062-0

Aller, R. C., N. E. Blair, Q. Xia, and P. D. Rude. 1996. Remineralization rates, recycling, and storage of carbon in amazon shelf sediments. Cont. Shelf Res. **16**: 753–786. doi:10.1016/0278-4343(95)00046-1

Almroth, E., A. Tengberg, J. H. Andersson, S. Pakhomova, and P. O. J. Hall. 2009. Effects of resuspension on benthic fluxes of oxygen, nutrients, dissolved inorganic carbon, iron and manganese in the Gulf of Finland, Baltic Sea. Cont. Shelf Res. **29**: 807–818. doi:10.1016/j.csr.2008.12.011

Berg, P., H. Røy, F. Janssen, V. Meyer, B. B. Jørgensen, M. Huettel, and D. De Beer. 2003. Oxygen uptake by aquatic sediments measured with a novel non-invasive eddy-correlation technique. Mar. Ecol. Prog. Ser. **261**: 75–83. doi:10.3354/meps261075

Berner, R. A. 1980. Early diagenesis: A theoretical approach. Princeton Univ. Press.

Bissett, A., C. Burke, P. L. M. Cook, and J. P. Bowman. 2007. Bacterial community shifts in organically perturbed sediments. Environ. Microbiol. **9**: 46–60. doi:10.1111/j.1462-2920.2006.01110.x

Boudreau, B. P., and B. B. Jørgensen. 2001. The benthic boundary layer: Transport processes and biogeochemistry. OUP USA.

Brand, A., C. Dinkel, and B. Wehrli. 2009. Influence of the diffusive boundary layer on solute dynamics in the sediments of a Seiche-Driven Lake: A model study. J. Geophys. Res. **114**: G01010. doi:10.1029/2008JG000755

Bryant, L. D., C. Lorrai, D. McGinnis, A. Brand, A. Wüest, and J. C. Little. 2010a. Variable sediment oxygen uptake in response to dynamic forcing. Limnol. Oceanogr. **55**: 950–964. doi:10.4319/lo.2010.55.2.0950

Bryant, L. D., D. F. McGinnis, C. Lorrai, A. Brand, J. C. Little, and A. Wüest. 2010b. Evaluating oxygen fluxes using microprofiles from both sides of the sediment-water interface. Limnol. Oceanogr.: Methods **8**: 610–627. doi:10.4319/lom.2010.8.610

Canfield, D. E., and others. 1993. Pathways of organic carbon oxidation in three continental margin sediments. Mar. Geol., Marine Sediments, Burial, Pore Water

Chemistry, Microbiology and Diagenesis, **113**: 27–40. doi:10.1016/0025-3227(93)90147-N

Chatelain, M., and K. Guizien. 2010. Modelling coupled turbulence—dissolved oxygen dynamics near the sediment–water interface under wind waves and sea swell. Water Res. **44**: 1361–1372. doi:10.1016/j.watres.2009.11.010

Chien, C. C., D. B. Blum, and G. A. Voth. 2013. Effects of fluctuating energy input on the small scales in turbulence. J. Fluid Mech. **737**: 527–551. doi:10.1017/jfm.2013.575

Dade, W. B. 1993. Near-bed turbulence and hydrodynamic control of diffusional mass transfer at the sea floor. Limnol. Oceanogr. **38**: 52–52. doi:10.4319/lo.1993.38.1.0052

Dean, W. E., Jr. 1974. Determination of carbonate and organic matter in calcareous sediments and sedimentary rocks by loss on ignition: Comparison with other methods. J. Sediment. Res. **44**: 242–248. doi:10.1306/74D729D2-2B21-11D7-8648000102C1865D

Edlund, A., F. Hårdeman, J. K. Jansson, and S. Sjöling. 2008. Active bacterial community structure along vertical redox gradients in Baltic Sea sediment. Environ. Microbiol. **10**: 2051–2063. doi:10.1111/j.1462-2920.2008.01624.x

Fanning, K. A., K. L. Carder, and P. R. Betzer. 1982. Sediment resuspension by coastal waters: A potential mechanism for nutrient re-cycling on the ocean's margins. Deep-Sea Res. Part A Oceanogr. Res. Pap. **29**: 953–965. doi:10.1016/0198-0149(82)90020-6

Fernando, H. J. S. 1991. Turbulent mixing in stratified fluids. Ann. Rev. Fluid Mech. **23**: 455–493. doi:10.1146/annurev.fl.23.010191.002323

Fincham, A. M., and Delerce. 2000. Advanced optimization of correlation imaging velocimetry algorithms. Exp. Fluids. **29**, S013–22. doi:10.1007/S003480070003

Frindte, K., W. Eckert, K. Attermeyer, and H. P. Grossart. 2013. Internal wave-induced redox shifts affect biogeochemistry and microbial activity in sediments: A simulation experiment. Biogeochemistry **113**: 423–434. doi:10.1007/s10533-012-9769-1

Froelich, P. N., and others. 1979. Early oxidation of organic matter in pelagic sediments of the eastern equatorial Atlantic: Suboxic diagenesis. Geochim. Cosmochim. Acta **43**: 1075–1090. doi:10.1016/0016-7037(79)90095-4

Gantzer, C. J., and H. G. Stefan. 2003. A model of microbial activity in lake sediments in response to periodic water-column mixing. Water Res. **37**: 2833–2846. doi:10.1016/S0043-1354(03)00110-6

Glud, R. N., J. K. Gundersen, N. P. Revsbech, B. B. Jorgensen, and M. Hüttel. 1995. Calibration and performance of the stirred flux chamber from the benthic lander Elinor. Deep-Sea Res. Part I Oceanogr. Res. Pap. **42**: 1029–1042. doi:10.1016/0967-0637(95)00023-Y

Glud, R. N., F. Wenzhöfer, A. Tengberg, M. Middelboe, K. Oguri, and H. Kitazato. 2005. Distribution of oxygen in surface sediments from central Sagami Bay, Japan: In situ measurements by microelectrodes and planar optodes. Deep-Sea Res. Part I Oceanogr. Res. Pap. **52**: 1974–1987. doi:10.1016/j.dsr.2005.05.004

Glud, R. N., P. Berg, H. Fossing, and B. B. Jorgensen. 2007. Effect of the diffusive boundary layer on benthic mineralization and O∼ 2 distribution: A theoretical model analysis. Limnol. Oceanogr. **52**: 547. doi:10.4319/lo.2007.52.2.0547

Glud, R. N., H. Stahl, P. Berg, F. Wenzhofer, K. Oguri, and H. Kitazato. 2009. In situ microscale variation in distribution and consumption of O2: A case study from a deep ocean margin sediment (Sagami Bay, Japan). Limnol. Oceanogr. **54**: 1–12. doi:10.4319/lo.2009.54.1.0001

Guizien, K., M. Dohmen-Janssen, and G. Vittori. 2003. 1DV bottom boundary layer modeling under combined wave and current: Turbulent separation and phase lag effects. J. Geophys. Res. **108**: 16–21. doi:10.1029/2001JC001292

Gundersen, J. K., and B. B. Jorgensen. 1990. Microstructure of diffusive boundary layers and the oxygen uptake of the sea floor. Nature **345**: 604–607. doi:10.1038/345604a0

Hannoun, L. A., and E. J. List. 1988. Turbulent mixing at a shear-free density interface. J. Fluid Mech. **189**: 211–234. doi: 10.1017/S0022112088000977

Higashino, M., C. J. Gantzer, and H. G. Stefan. 2004. Unsteady diffusional mass transfer at the sediment/water interface: Theory and significance for SOD measurement. Water Res. **38**: 1–12. doi:10.1016/j.watres.2003.08.030

Higashino, M., and H. Stefan. 2005. Oxygen demand by a sediment bed of finite length. J. Environ. Eng. **131**: 350–358. doi:10.1061/(ASCE)0733-9372(2005)131:3(350)

Holtappels, M., M. M. M. Kuypers, M. Schlüter, and V. Brüchert. 2011. Measurement and interpretaion of solute concentration gradients in the benthic boundary layer. Limnol. Oceanogr.: Methods **9**: 1–13. doi:10:4319/lom.2011.9.1

Hondzo, M., T. Feyaerts, R. Donovan, and B. L. O'Connor. 2005. Universal scaling of dissolved oxygen distribution at the sediment-water interface: A power law. Limnol. Oceanogr. **50**: 1667–1676. doi:10.4319/lo.2005.50.5.1667

Hopfinger, E. J., and J.-A. Toly. 1976. Spatially decaying turbulence and its relation to mixing across density interfaces. J. Fluid Mech. **78**: 155–175. doi:10.1017/S0022112076002371

House, W. A. 2003. Factors influencing the extent and development of the oxic zone in sediments. Biogeochemistry **63**: 317–334. doi:10.1023/A:1023353318856

Huettel, M., and G. Gust. 1992. Impact of bioroughness on interfacial solute exchange in permeable sediments." Mar. Ecol. Prog. Ser. Oldendorf **89**: 253–267. doi:10.3354/meps089253

Huettel, M., W. Ziebis, and S. Forster. 1996. Flow-induced uptake of particulate matter in permeable sediments. Limnol. Oceanogr. **41**: 309–322. doi:10.4319/lo.1996.41.2.0309

Huppert, H. E., J. S. Turner, and M. A. Hallworth. 1995. Sedimentation and entrainment in dense layers of suspended

particles stirred by an oscillating grid. J. Fluid Mech. **289**: 263–293. doi:10.1017/S0022112095001339

Hutchinson, G. E. 1957. Concluding remarks. Cold Spring Harbor Symposia on Quantitative Biology **22**: 415–427. doi:10.1101/SQB.1957.022.01.039

Jorgensen, B. B., and D. J. Des Marais. 1990. The diffusive boundary layer of sediments: Oxygen microgradients over a microbial mat. Limnol. Oceanogr. **35**: 1343–1355. doi:10.4319/lo.1990.35.6.1343

Kline, S. J., W. C. Reynolds, F. A. Schraub, and P. W. Runstadler. 1967. The structure of turbulent boundary layers. J. Fluid Mech. **30**: 741–773. doi:10.1017/S0022112067001740

Lorke, A., B. Muller, M. Maerki, and A. Wuest. 2003. Breathing sediments: The control of diffusive transport across the sediment-water interface by periodic boundary-layer turbulence. Limnol. Oceanogr. **48**: 2077–2085. doi:10.4319/lo.2003.48.6.2077

Manheim, F. T., and L. S. Waterman. 1974. Porosity, density, grain density, and related physical properties of sediments from the Red Sea drill cores, p. 887–907. Initial reports of the Deep Sea Drilling Project XXIII, R. B. Whitmarsh, and others [eds.] U.S. Government Printing Office, Washington Reports of the Deep Sea Drilling Project XXII.

Medina, P., M. A. Sánchez, and J. M. Redondo. 2001. Grid stirred turbulence: Applications to the initiation of sediment motion and lift-off studies. Phys. Chem. Earth Part B Hydrol. Oceans Atmos. **26**: 299–304. doi:10.1016/S1464-1909(01)00010-7

Morse, J. W., and P. M. Eldridge. 2007. A non-steady state diagenetic model for changes in sediment biogeochemistry in response to seasonally hypoxic/anoxic conditions in the 'dead Zone' of the Louisiana shelf. Mar. Chem. **106**: 239–255. doi:10.1016/j.marchem.2006.02.003

Munk, W., and C. Wunsch. 1998. Abyssal recipes II: Energetics of tidal and wind mixing. Deep-Sea Res. Part I Oceanogr. Res. Pap. **45**: 1977–2010. doi:10.1016/S0967-0637(98)00070-3

O'Connor, B. L., and M. Hondzo. 2008. Dissolved oxygen transfer to sediments by sweep and eject motions in aquatic environments. Limnol. Oceanogr. **53**: 566. doi:10.4319/lo.2008.53.2.0566

Rasmussen, H., and B. B. Jørgensen. 1992. Microelectrode studies of seasonal oxygen uptake in a coastal sediment: Role of molecular diffusion. Mar. Ecol. Prog. Ser. Oldendorf **81**: 289–303. doi:10.3354/meps081289

Redondo, J. M. 1988. Difusión turbulenta por rejilla oscilante. Revista de Geofísica **44**: 163–174.

Redondo, J. M., X. Durrieu de Madron, P. Medina, M. A. Sanchez, and E. Schaaff. 2001. Comparison of sediment resuspension measurements in sheared and zero-mean turbulent flows. Cont. Shelf Res., European Land-Ocean Interaction **21**: 2095–2103. doi:10.1016/S0278-4343(01)00044-9

Revsbech, N. P. 1989. An oxygen microsensor with a guard cathode. Limnol. Oceanogr. **34**: 474–478. doi:10.4319/lo.1989.34.2.0474

Roy, H., M. Huettel, and B. B. Jorgensen. 2004. Transmission of oxygen concentration fluctuations through the diffusive boundary layer overlying aquatic sediments. Limnol. Oceanogr. **49**: 686–692. doi:10.4319/lo.2004.49.3.0686

Stahlberg, C., D. Bastviken, B. H. Svensson, and L. Rahm. 2006. Mineralisation of organic matter in coastal sediments at different frequency and duration of resuspension. Estuar. Coast. Shelf Sci., Applying the Ecohydrology approach to the Guadiana estuary and coastal areas: lessons learned from dam impacted ecosystems **70**: 317–325. doi:10.1016/j.ecss.2006.06.022

Steinberger, N., and M. Hondzo. 1999. Diffusional mass transfer at sediment-water interface. J. Environ. Eng. **125**: 192–200. doi:10.1061/(ASCE)0733-9372(1999)125:2(192)

Tengberg, A., and others. 1995. Benthic chamber and profiling landers in oceanography—a review of design, technical solutions and functioning. Prog. Oceanogr. **35**: 253–294. doi:10.1016/0079-6611(95)00009-6

Tengberg, A., H. Stahl, G. Gust, V. Müller, U. Arning, H. Andersson, and P. O. J. Hall. 2004. Intercalibration of benthic flux chambers I. Accuracy of flux measurements and influence of chamber hydrodynamics. Prog. Oceanogr. **60**: 1–28. doi:10.1016/j.pocean.2003.12.001

Thorpe, S. A. 2005. The turbulent ocean. Cambridge Univ. Press.

Turner, J. S. 1968. The influence of molecular diffusivity on turbulent entrainment across a density interface. J. Fluid Mech. **33**: 639–56. doi:10.1017/S002211206800159X

Ullman, W. J., and R. C. Aller. 1982. Diffusion coefficients in nearshore marine sediments. Limnol. Oceanogr. **27**: 552–556. doi:10.4319/lo.1982.27.3.0552

Wainright, S. C., and C. S. Hopkinson, Jr. 1997. Effects of sediment resuspension on organic matter processing in coastal environments: A simulation model. J. Mar. Syst. **11**: 353–368. doi:10.1016/S0924-7963(96)00130-3

Acknowledgments

We would like to thank proof-reading-service.com for correcting the English. This work is in partial fulfillment of the Ph.D. Thesis of Sabrina Lucas who was supported by a doctoral fellowship from the French National Center for Scientific Research (CNRS). This work was funded by the French National Program for Continental and Coastal Ecosphere (EC2CO) under project DynDiagHyd – Diagenesis dynamics in aquatic sediments under unsteady hydrodynamics (PI K. Guizien).

Submitted 19 January 2015
Revised 24 July 2015
Accepted 13 August 2015

Associate editor: John Crimaldi